

Mixture of ultracold lithium and cesium atoms in an optical dipole trap

A. Mosk, S. Kraft, M. Mudrich, K. Singer, W. Wohlleben*, R. Grimm**, and M. Weidmüller

Max-Planck-Institut für Kernphysik, 69029 Heidelberg, Germany

Received: date / Revised version: date

Abstract We present the first simultaneous trapping of two different ultracold atomic species in a conservative trap. Lithium and cesium atoms are stored in an optical dipole trap formed by the focus of a CO₂ laser. Techniques for loading both species of atoms are discussed and observations of elastic and inelastic collisions between the two species are presented. A model for sympathetic cooling of two species with strongly different mass in the presence of slow evaporation is developed. From the observed Cs-induced evaporation of Li atoms we estimate a cross section for cold elastic Li-Cs collisions.

1 Introduction

Mixtures of ultracold atoms add many new possibilities to the study of interactions in ultracold gases since the different components of the mixture can have widely different intrinsic properties, e.g., different masses, spins, scattering properties and quantum statistics. On one hand, many interesting phenomena are exclusive to gas mixtures, such as mixing and de-mixing phenomena [1, 2], the subtle interplay between bosonic and fermionic atoms [3], or the prospect of forming ultracold heteronuclear molecules through photoassociation [4]. On the other hand, one may see an atomic gas mixture as a tool for transferring the favorable thermodynamic properties of one component (low temperature, high magnetization) to the other component. In this case one would like to use one gas that is easy to cool or polarize, and bring it in contact with a second gas that is harder to handle. These processes are commonly referred to as sympathetic cooling and polarization exchange.

* Present address: Max-Planck-Institut für Quantenoptik, 85748 Garching, Germany

** Permanent address: Institut für Experimentalphysik, Universität Innsbruck, A-6020 Innsbruck, Austria

Already 15 years ago, cryogenically cooled helium was used as a buffer gas to precool and load atomic hydrogen into a magnetic trap [5]. More recently, this method was extended to other atomic species and even molecules [6]. Sympathetic cooling with ultracold, trapped gases has initially been studied for different *hyperfine* states of evaporatively cooled rubidium atoms in order to create two overlapping Bose-Einstein Condensates (BECs) [7]. Later, evaporative cooling of a mixture of *magnetic spin* states was employed as the key step to create a degenerate Fermi gas of fermionic ⁴⁰K [8]. Most recently, sympathetic cooling in magnetic traps has been applied to different *isotopes* of the same atomic species: the bosonic species ⁸⁵Rb cooled by ⁸⁷Rb [9] and the fermionic ⁶Li cooled by ⁷Li [10,11]. So far, no experiments are reported which investigate elastic interactions in two distinct atomic *species*.

Sympathetic cooling of a mixture of different atomic species in principle offers an enormous advantage if one species can be optically cooled to much lower temperatures than the other. We are investigating a mixture of the alkaline atoms lithium and cesium. This combination represents the prototype of a mixture in which one component (lithium) is hard to cool optically while the other (cesium) allows sub-Doppler temperatures ($< 3 \mu\text{K}$ in free space) to be reached by simple polarization-gradient cooling. In contrast to evaporative cooling, the cooling process does not lead to a significant loss of either the cooled gas or the cooling agent. Sympathetic cooling with cesium (or other sub-Doppler cooled atoms) may be the method of choice for cooling many other atomic and molecular species, including LiCs molecules formed by photoassociation from the same mixed-species sample!

We present the first observation of simultaneous trapping of two different atomic species in a conservative trap: lithium and cesium atoms stored in a very far-detuned optical dipole trap. Our optical trap is based on a CO₂ laser emitting light at 10.6 μm [17]. The trap provides a conservative potential which is independent of

the hyperfine state and spin projection of the atoms [18]. This allows us to study exoergic spin exchange collisions as well as elastic interactions. Exoergic collisions between different species have been previously investigated in light-pressure traps [12, 13, 14] but the near-resonant light is known to influence the cross-sections even for collisions involving only the ground state [15]. No previous measurements of two-species collision cross-sections in conservative traps exist. If all atoms are in the lower hyperfine state, exoergic collisions are impossible. We nevertheless see slow evaporation of lithium, which is an indication that thermalization through elastic collisions is taking place. To interpret this evaporation and to estimate a collision cross section from it, we adapt a model given in Ref. [16] and we develop a rate equation model for sympathetic cooling with slow evaporation.

This paper is organized as follows: An overview of the apparatus is given in section 2 and the methods for loading and characterization of the trap are discussed in section 3. The exoergic spin-changing collisions are studied in section 4. Finally, a rate equation model for sympathetic cooling is given in section 5, and compared to numerical results and experimental data.

2 Quasi-electrostatic trap

The focus of a CO₂ laser beam constitutes an almost perfect realization of a conservative trapping potential for atoms. The atoms experience an optical dipole force which points towards the maximum of the intensity thus providing stable confinement in all spatial directions. Since the frequency of the CO₂ laser is far below any dipole-allowed atomic transition frequency, the induced atomic dipole moment oscillates in phase with the oscillating electric field of the laser as if the field was a slowly varying static field. Therefore, the name quasi-electrostatic trap (QUEST) has been coined for this particular realization of an optical dipole trap. Due to the large detuning of the laser frequency from any atomic resonances, heating through photon scattering can be completely neglected.

For an intensity distribution $I(\mathbf{r})$ the potential $U(\mathbf{r})$ is given by $U(\mathbf{r}) = -\alpha_{\text{stat}}I(\mathbf{r})/2\varepsilon_0c$ where α_{stat} denotes the static polarizability of the atoms [17, 18]. For a focused beam of power P and waist w one gets a trap depth $\epsilon_t = 2\alpha_{\text{stat}}P/(\pi\varepsilon_0cw^2)$. We employ an industrial, sealed-tube CO₂ laser (Synrad Evolution) providing 140 W of power in a nearly TEM₀₀ transversal mode characterized by $M^2 = 1.2$. The laser beam is first expanded by a telescope, and then focused into the vacuum chamber by a lens of 254 mm focal length. The focus has a waist of 85 μm , yielding a trap depth of 390 μK for Li and 1000 μK for Cs (in units of the Boltzmann constant k_{B}). Assuming a pure Gaussian beam, one finds a Rayleigh range z_{R} of 1.5 mm. The axial and radial oscillation frequencies in the harmonic approximation are given by

$\omega_z = (2U_0/mz_{\text{R}}^2)^{1/2}$ and $\omega_r = (4U_0/mw^2)^{1/2}$ with m denoting the mass of the atom.

Fig. 1 shows a schematic view of the apparatus. Atoms are transferred into the dipole trap from magneto-optical traps (MOT) for lithium and cesium which are superimposed on the focus of the CO₂ laser beam. Both MOTs are loaded from atomic beams that are cooled and decelerated by decreasing-field Zeeman slowers which use the fringe fields of the MOT magnetic quadrupole field for the final deceleration stage. Fluorescence of the atoms in the MOT is detected by photodiodes with appropriate filters to discriminate the resonance fluorescence of Li at 671 nm from the fluorescence of cesium at 852 nm. The main vacuum chamber at a background pressure of about 6×10^{-11} mbar is connected to the oven chambers by tubes which are divided into differentially-pumped sections. Both atomic beams can be interrupted by mechanical shutters.

3 Storage in the quasi-electrostatic trap

3.1 Cesium

To load cesium into the QUEST, a cloud of typically 10^7 atoms is first accumulated in the MOT with a quadrupole field gradient of 26 G/cm along the symmetry axis. The atoms are further compressed and cooled by decreasing the detuning of the MOT trapping laser from initially $-2\Gamma_{\text{Cs}}$ to $-25\Gamma_{\text{Cs}}$ with respect to the $6^2\text{S}_{1/2}(F=4)$ - $6^2\text{P}_{3/2}(F=5)$ transition (natural linewidth $\Gamma_{\text{Cs}}/2\pi = 5.3$ MHz). After 5 ms of compression, the distribution of atoms in the MOT has a rms radius of 400 μm corresponding to a mean density of about 10^{10} atoms/cm³. After the compression, the magnetic field of the MOT is turned off, and the atoms are further cooled in a blue optical molasses [19] by detuning the laser field to $+2\Gamma_{\text{Cs}}$ with respect to the $6^2\text{S}_{1/2}(F=4)$ - $6^2\text{P}_{3/2}(F=4)$ transition for 20 ms.

The CO₂ laser beam is present during the whole loading phase. Since the static polarizability of the $6^2\text{P}_{3/2}$ state in cesium is larger than the polarizability of the ground state by around a factor of 4, the atomic resonance frequency of the cesium D2 line is inhomogeneously shifted with a maximum value of roughly $-10\Gamma_{\text{Cs}}$. However, the number of atoms in the MOT is found to be independent of whether the CO₂ is turned on or off.

After the cooling laser beams have been turned off, up to 10^6 atoms remain trapped in the focus of the CO₂ laser beam at a temperature of 30 μK and a peak density close to 10^{12} atoms/cm³. Atoms are prepared in either the $F=3$ or the $F=4$ hyperfine ground state by shutting the cooling laser 1 ms after or before the repumping laser has been shuttered, respectively. To detect the optically trapped atoms, we either recapture the atoms in the MOT and measure the intensity of the fluorescence light, or we analyze the spatially resolved absorption of a

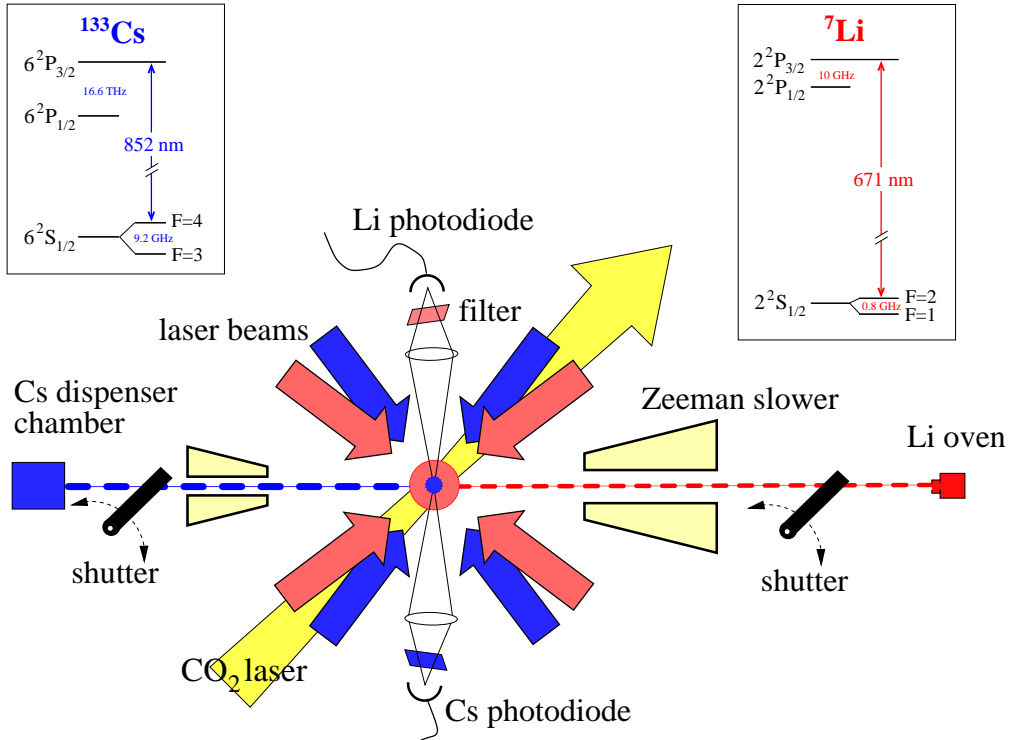


Fig. 1 Schematic setup of the experiment. The insets show the relevant energy levels of lithium and cesium.

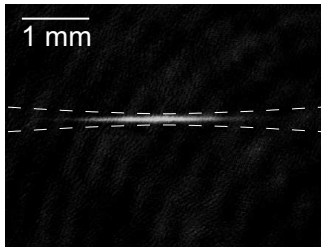


Fig. 2 Absorption image of cesium atoms in the QUEST. The dashed lines indicate the profile of the CO_2 laser beam

weak resonant probe beam passing through the trapped atoms (absorption imaging [20]). The latter method allows one to absolutely calibrate the atom number. In Fig. 2, the absorption image of the trapped Cs atoms shows the expected elongated shape with an aspect ratio of $\omega_{\text{ax}}/\omega_{\text{rad}} \simeq 44$. Note, that the radial extension of the atomic cloud is not resolved by our camera system.

The evolution of the number of atoms in the dipole trap is measured by recapturing the atoms back into the MOT after a variable storage time. The number of atoms is determined from a charge coupled device camera picture by integrating over the fluorescence image, while subtracting a background image. We expect the particle number determined by this method to be accurate within a factor of two. Fluctuations in the loading flux are cancelled by loading the MOT up to a certain density (determined by the fluorescence signal) rather than for a fixed period of time: A photodiode records the fluorescence of the atoms in the MOT and triggers the transfer

cycle as soon as it exceeds a predefined discriminator level. The decay of the number of stored cesium atoms is shown in Fig. 3(a) from which one infers a $1/e$ storage time of 150 s. The very long storage time is purely limited by collisions with hot atoms out of the background gas at the base pressure of 6×10^{-11} mbar in our vacuum chamber [22]. Laser-noise induced loss mechanisms [21] can apparently be completely neglected. Since Cs has a large scattering length the Cs gas thermalizes on a time scale of < 0.1 s. In contrast to previous experiments in a shallower trap [22], spontaneous evaporation of atoms is exponentially suppressed by a factor $\eta \equiv \epsilon_t/k_B T$ of more than 20. Experimentally, we indeed observe neither loss of Cs atoms nor reduction of the temperature due to evaporation.

To determine the characteristic frequencies of the trap, we induce axial and radial oscillations of the cloud of trapped atoms. Radial oscillations are excited by a release-recapture cycle in the optical trap. First, the laser is turned off (switch-off time $< 100 \mu\text{s}$) which leads to a ballistic expansion of the atomic cloud. After ~ 0.5 ms, the cloud has expanded to about twice its initial radial width. Then, the CO_2 laser is turned on again and almost all atoms are recaptured by the dipole trap. Through this process, the atoms have gained potential energy, which is subsequently converted into kinetic energy. Thus, the radial size of the atom cloud starts to oscillate at twice the radial oscillation frequency. Since we can not fully resolve the radial extension of the atom cloud with our absorption imaging system, we measure

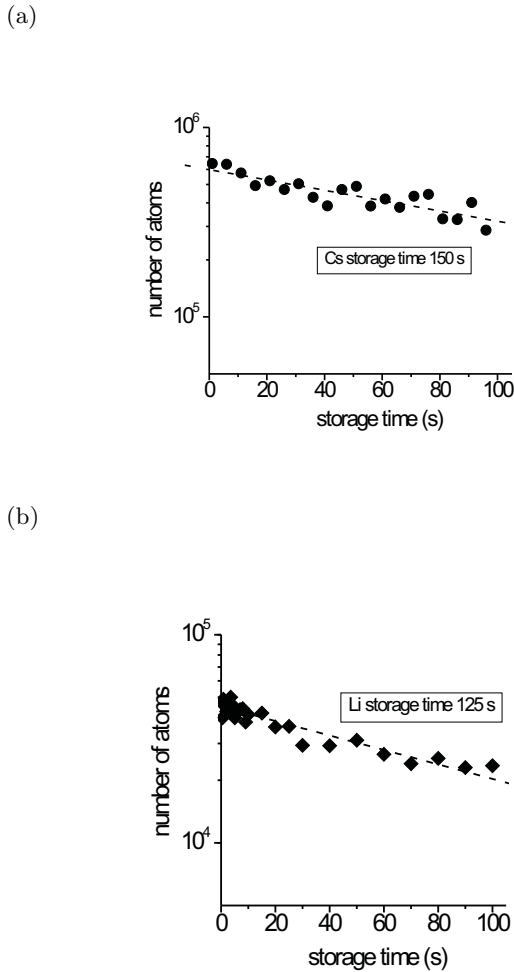


Fig. 3 Very long storage times for (a) cesium and (b) lithium in the quasi-electrostatic trap. The atoms are optically pumped into the lowest ground state. The corresponding $1/e$ lifetimes are 150 ± 15 s for cesium and 125 ± 15 s for lithium.

the corresponding oscillation in the kinetic energy. For this purpose, the CO₂ laser is turned off again after a variable delay relative to the release-recapture cycle, and the radial extension is determined through absorption imaging after 1.2 ms of ballistic expansion. Fig. 4(a) shows the oscillation of the root mean square velocity at a frequency of 1.6 kHz. The corresponding oscillation frequency of the trapped atoms of 0.8 kHz is in reasonable agreement with the expected radial oscillation frequency for a focused beam with a waist of 85 μ m.

Axial oscillations can easily be excited by loading at an axial position off the focus. For this purpose, the relative position of the MOT is shifted along the propagation direction of the CO₂-laser beam. After transfer into the QUEST, the cesium cloud starts to perform a damped oscillation at a frequency of 18 Hz as depicted in the upper graph of Fig. 4. The damping of the oscillation is caused by the anharmonicity of the confining potential.

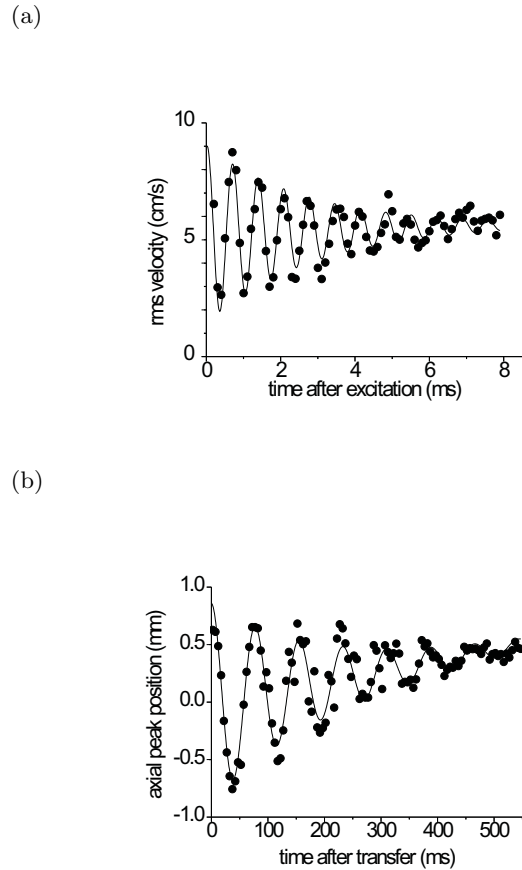


Fig. 4 Measurement of (a) radial, and (b) axial oscillations of Cs atoms in the quasi-electrostatic trap. The solid lines show the fits to a damped sinusoidal oscillation. For the axial oscillation, a constant drift of the focus position was included into the fit.

	trap depth	radial frequency	axial frequency
Lithium	390 μ K	50 Hz	2.2 kHz
Cesium	1000 μ K	18 Hz	0.8 kHz

Table 1 Parameters of the quasi-electrostatic trap for lithium and cesium. The Li frequencies are calculated from the measured Cs frequencies.

Assuming a pure Gaussian beam, one would expect an oscillation frequency about twice as large as the actual measured value. We explain the discrepancy by aberrations in the optical system. Table 3.1 summarizes the relevant trap parameters for lithium and cesium.

In the first few seconds after the CO₂ laser has been turned on, we observe a small drift of the axial position of the laser focus, which can be attributed to thermal effects in the laser cavity and optics. To eliminate this drift of the focal position, we leave the CO₂ laser permanently on while loading the MOT and transferring the atoms.

3.2 Lithium

For cesium the thermal energy of the atoms in the MOT is much smaller than the depth of the QUEST which results in a rather large transfer efficiency. The situation is different for lithium. Due to the large recoil of photons on lithium atoms, the thermal energies in a lithium MOT are comparable or even larger than the depth of the dipole trap resulting in a poor phase-space overlap and thus a small transfer efficiency.

The lithium MOT is also loaded from a Zeeman-slowed atomic beam. Details of the MOT system are described in Ref. [23]. The largest numbers of Li atoms are accumulated at relatively large detunings of the MOT lasers acting on the two hyperfine components of the Li $D2$ line. After loading typically 10^7 atoms into the MOT, the atomic cloud is compressed for 4 ms by switching the detunings closer to resonance ($-1\Gamma_{\text{Li}}$ with $\Gamma_{\text{Li}}/2\pi = 5.9$ MHz). Due to the unresolved hyperfine structure of the excited state, sub-Doppler cooling mechanisms are inefficient for lithium and temperature is essentially determined by the limit for Doppler cooling ($140\mu\text{K}$ at low saturation). To attain a temperature close to that limit, the MOT magnetic field is turned off and the MOT lasers are attenuated to 20% of their full power which leads to a final temperature of $350\mu\text{K}$ and a cloud size of $800\mu\text{m}$ after typically 1 ms. In contrast to cesium, the light shift of the CO_2 laser beam on the $D2$ resonance line is negligible since the static polarizability of the ground and excited state differ by only 25%.

After all MOT laser beams have been shut off, about 0.5% of the Li atoms are captured by the QUEST with a peak density of $\sim 10^{10}$ atoms/cm 3 . Thermalization of these atoms is extremely slow: estimated collision times based on the s-wave scattering lengths for Li are exceeding 100 seconds. On the time scales of the experiments discussed in the following, lithium can therefore not be assumed to be in thermal equilibrium.

Due to the small optical density of the sample, we were so far not able to directly measure the distribution of lithium atoms in the trap by absorption imaging techniques. Instead, we have performed a Monte-Carlo simulation of the transfer process which provides us with the spatial and energy distributions. The energy distribution is highly non-thermal with most atoms populating high lying energy states in the potential because of the large initial thermal energy relative to the trap depth. The small rate for elastic collisions inhibits evaporation of these loosely bound atoms. The measurement of the number of trapped lithium atoms as a function of storage time depicted in Fig. 3 thus shows a pure exponential decay with a time constant of 125 s with no indication for evaporation of particles from the trap. On the basis of the above estimate for the thermalization times, we assume the energy distribution hardly changes with time.

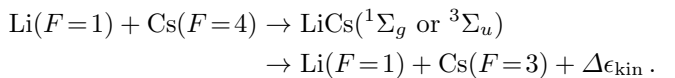
3.3 Combined transfer

To load a mixture of lithium and cesium, one could start from a two-species MOT [14], but in this case the numbers of atoms and the densities are severely limited by light-assisted inelastic collisions between the two species. However, our measurements with a 2-species MOT showed that collisions involving optically excited Li (Li^*) and ground-state Cs are strongly suppressed by optical shielding through the repulsive van-der-Waals interaction in the Li^* -Cs manifold [14]. It is therefore favorable to first optically cool and transfer Cs into the QUEST, and then load the Li MOT. A typical loading time of the Li MOT is 4 s. In order to exclude any loss processes by inelastic collisions, we spatially separate the Li MOT from the optically trapped Cs sample with a small bias magnetic field (3 G) shifting the centre of the Li MOT by about 2 mm. In this way, we observe no loss of Li and only a 50 % loss of Cs in the combined transfer, as compared to the separate trapping of only one species. A detailed investigation of the combined transfer will be published elsewhere.

4 Spin-changing lithium-cesium collisions

Two atoms approaching each other in their electronic ground state may either collide elastically with the total energy being conserved, as will be discussed in the next Section, or they may undergo an exoergic collision transforming internal energy into kinetic energy of the collision partners. The latter process leads to trap loss if the kinetic energy release is larger than the escape energy of the trap. Optical dipole traps are perfectly suited to study inelastic processes among trapped atoms since the optical trapping force is conservative with a well-defined potential, the investigation may be performed in zero magnetic field or in a controlled homogeneous field, and the atoms can be prepared in any internal state by appropriate optical pumping methods. Up to now, no experiment on ultracold inelastic collisions between two different atomic species in the electronic ground state has reported.

For ground-state Li and Cs atoms in an optical dipole trap, the essential inelastic processes are collisions that change the hyperfine quantum numbers F and m_F . The spin-changing collision process between lithium and cesium can be written symbolically as



The potential curves for the singlet and triplet ground states of the Li-Cs pair are schematically depicted in Fig. 5. Spin-changing collisions exiting at a lower energetic asymptote than the entrance channel lead to a transformation of the internal energy into kinetic energy $\Delta\epsilon_{\text{kin}}$ of the collision partners, and consequently to loss

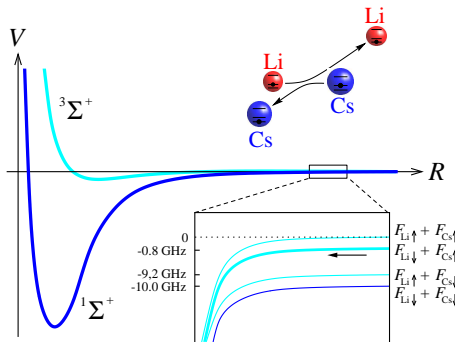


Fig. 5 Ground-state potential energy curves for the heteronuclear dimer LiCs. The main plot shows the potential energy V (y-axis) versus distance R (x-axis). It features two curves: a blue curve for the $1\Sigma^+$ state and a cyan curve for the $3\Sigma^+$ state. The $1\Sigma^+$ curve has a deep well, while the $3\Sigma^+$ curve is shallower. An inset shows an enlargement at long range, with two atoms (Li and Cs) represented as spheres. The Cs atom has two hyperfine levels, indicated by blue and red shading. The inset also shows five energy levels for the dimer: $F_{\text{Li}}\uparrow + F_{\text{Cs}}\uparrow$, $F_{\text{Li}}\downarrow + F_{\text{Cs}}\uparrow$, $F_{\text{Li}}\uparrow + F_{\text{Cs}}\downarrow$, $F_{\text{Li}}\downarrow + F_{\text{Cs}}\downarrow$, and $F_{\text{Li}}\uparrow + F_{\text{Cs}}\downarrow$. An arrow points to the $F_{\text{Li}}\uparrow + F_{\text{Cs}}\uparrow$ level, indicating the incoming channel.

from the trap. Although lithium takes the major share of the kinetic energy gain, both atoms escape from the QUEST due to the small trap depth as compared to the hyperfine energy.

Inelastic collisions of trapped ground-state atoms have been extensively studied theoretically and experimentally since the early days of magnetic traps [24]. Hyperfine-changing collisions represent the major limitation on achievable densities and/or storage times in magnetic traps. These collisions in magnetic traps are almost unavoidable, since atoms can not be trapped in the lowest energetic state. In particular, spin-changing collisions impede sympathetic cooling between different atomic species in magnetic traps.

Exoergic ground-state collisions also turned out to be an important loss mechanism in shallow light-pressure traps. They were observed and analyzed for homonuclear collisions [25], as well as for mixtures of different elements [12,13,14]. However, as has been pointed out recently [15], the presence of near-resonant light strongly modifies the dynamics of the collision process which can lead to a dramatic change in the measured rate coefficients. Therefore, care should be taken to interpret trap loss and the corresponding rate coefficients in shallow light-pressure traps as an indication of pure ground-state collisions. In a purely conservative trap such as the QUEST the situation is much better defined since the trapping light has negligible influence on the collision process.

To qualitatively investigate whether hyperfine-changing collisions between Li and Cs can be observed with the particle numbers and densities available in our QUEST, we have pumped one of the species into the upper hyperfine ground state and recorded the effect on the storage time of the other species, which was prepared in the lower hyperfine state. The result of these experiments is depicted in Fig. 6. From the timescale of the graph it immediately becomes apparent, that the presence of a hyperfine-excited atomic gas reduces the storage time of

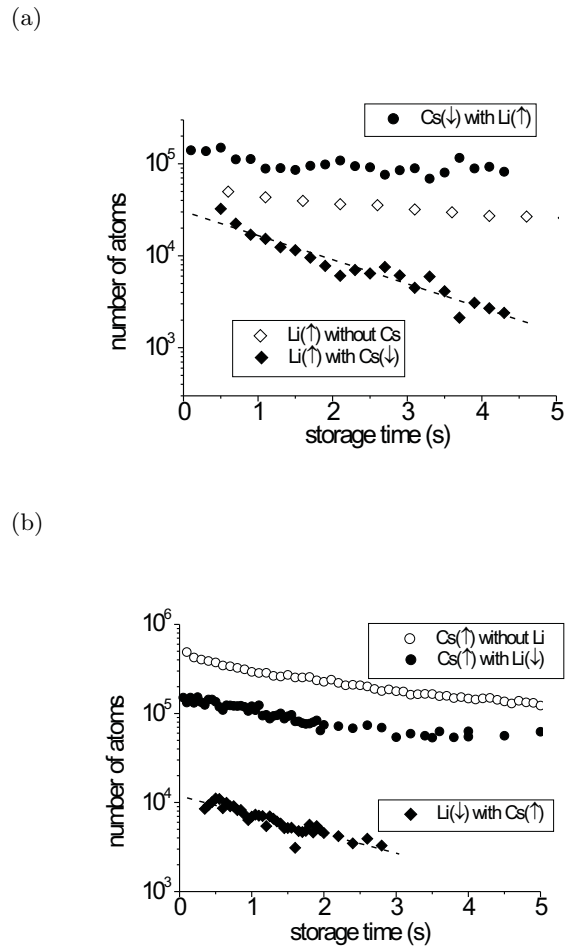


Fig. 6 Exoergic spin-changing collisions between lithium and cesium resulting in trap loss. (a): Li $2^2S_{1/2}(F_{\text{Li}}\uparrow=2)$ and Cs $6^2S_{1/2}(F_{\text{Cs}}\downarrow=3)$. (b): Li $2^2S_{1/2}(F_{\text{Li}}\downarrow=1)$ and Cs $6^2S_{1/2}(F_{\text{Cs}}\uparrow=4)$. Here, \uparrow stand for the upper hyperfine ground state and \downarrow stands for the lowest-energy hyperfine state. The dashed lines indicate the fit to an exponential decay yielding a time constant of 1.7 s and 1.9 s for the upper and lower graph, respectively.

the species in the lowest energetic state by more than an order of magnitude as compared to the rest-gas limited lifetimes (see Fig. 3).

In Fig. 6(a), we show data for a combination of Li in the upper hyperfine state [Li $2^2S_{1/2}(F_{\text{Li}}\uparrow=2)$], with Cs in the lower hyperfine ground state [Cs $6^2S_{1/2}(F_{\text{Cs}}\downarrow=3)$]. Without the presence of Cs, the Li slowly decays through exoergic Li-Li collisions. The effect of collision with restgas atoms can be neglected on this timescale. In presence of Cs, the Li decay is much faster. Spin-exchange between Li and Cs atoms is the dominant process for these interspecies collisions. An enhanced Li-Li inelastic collision rate due to an increased Li density after thermalization with the Cs may also play a minor role, but this would lead to a non-exponential decay of the Li, while we observe an exponential decay with a

time constant of 1.7 s. The effect of spin-changing Li-Cs collisions on the Cs is not observable as the Cs atoms outnumber the Li atoms. As the lithium distribution is not known, and may even be nonconstant due to elastic collisions happening simultaneously, we can currently only estimate the order of magnitude of the inelastic rate constant $\beta_{\text{Cs}\downarrow\text{Li}\uparrow} \sim 10^{-10} \text{ cm}^3/\text{s}$. We are currently implementing an improved absorption imaging system for Li in our apparatus, which will allow us to measure the density distribution of the Li atoms and thus allow for quantitative measurements of the rate coefficients.

In Fig. 6(b), we investigate the influence of Cs in the upper hyperfine ground state [Cs $6^2S_{1/2}(F_{\text{Cs}\uparrow}=4)$] on Li in the lower hyperfine state [Li $2^2S_{1/2}(F_{\text{Li}\downarrow}=1)$]. Cs itself decays due to exoergic Cs-Cs collisions. The Li, however, is lost on a much shorter timescale of 2 s. Due to the unknown Li distribution, we can only offer an estimate of the rate constant of the exoergic collisions of $\beta_{\text{Cs}\uparrow\text{Li}\downarrow} = \sim 10^{-10} \text{ cm}^3/\text{s}$. As one might expect, both rate constants are of the same order of magnitude.

5 Sympathetic cooling with slow sympathetic evaporation

In case both atomic gases are in the lower hyperfine states [Li $2^2S_{1/2}(F_{\text{Li}\downarrow}=1)$ and Cs $6^2S_{1/2}(F_{\text{Cs}\downarrow}=3)$], only elastic collisions are possible. These collisions lead to energy transfer between the distributions, which in turn leads to two different phenomena: The most obvious one is the equalization of the temperatures of the two gases, which is referred to as sympathetic cooling. A second phenomenon is the evaporative loss of one or both species through collisions with the other species, which we call sympathetic evaporation.

5.1 Sympathetic cooling

For the case where all relevant temperatures are well below the trap depth, the dynamics are relatively simple: No atoms evaporate and the temperatures of the two components approach each other. A quantum-mechanical treatment of sympathetic cooling has been given in Refs. [26, 27]. For the Boltzmann regime, an analytical formula for the evolution of the temperatures in a mixture of equal mass atoms was derived in Ref. [16]. In the same paper, the approach is extended towards atoms with different mass, however, the dependence of the cooling efficiency on the mass ratio is derived under the assumption of equal trap frequencies. This assumption corresponds to an implicit mass dependence of the trap potential, which is not present for realistic traps, and which leads to a strongly overestimated reduction of the cooling efficiency at large mass ratio. Below, we adapt the approach of Ref. [16] by assuming an explicit trap potential, so that our results remain valid for large mass ratios. The average energy transfer per collision can be calculated from

simple kinematics,

$$\Delta E_{1\rightarrow 2} = \xi k_B(T_1 - T_2); \quad \xi \equiv \frac{4m_1m_2}{(m_1 + m_2)^2}. \quad (1)$$

The energy transfer is reduced by a factor ξ with respect to collisions between atoms with equal mass. For equal mass atoms in a harmonic trap, approximately 3 collisions are needed for thermalization (see [16] and references therein), as the heat capacity per atom is $3k_B$. For ^{133}Cs and ^7Li , we need $3/\xi \approx 15$ collisions to thermalize.

The Cs-Li collision rate depends on the spatial overlap between the thermal distributions,

$$I_{\text{coll}} = \sigma_{12}\bar{v} \int d^3x n_1(\mathbf{x})n_2(\mathbf{x}) \quad (2)$$

Here \bar{v} is the mean thermal relative velocity,

$$\bar{v} = \left[\frac{8k_B}{\pi} \left(\frac{T_1}{m_1} + \frac{T_2}{m_2} \right) \right]^{1/2} \quad (3)$$

We assume a harmonic trapping potential, $V_i(\mathbf{x}) = (\boldsymbol{\alpha}_i \cdot \mathbf{x})^2$, where $i = 1, 2$, and $\boldsymbol{\alpha}_i$ is a species-dependent vector of force constants. We will assume the trap constants are linearly dependent, i.e. $\boldsymbol{\alpha}_2 = \beta \boldsymbol{\alpha}_1 = \beta \boldsymbol{\alpha}$. This allows us to write the collision rate as

$$I_{\text{coll}} = \frac{\sigma_{12}\bar{v}N_1N_2}{\pi^{3/2}k_B^{3/2}} \alpha_x \alpha_y \alpha_z (T_1 + T_2\beta^{-2})^{-3/2}. \quad (4)$$

The timescale of thermalization can be obtained from the differential equation for $\Delta T = T_2 - T_1$:

$$\tau^{-1} = \frac{d(\Delta T)}{\Delta T dt} = \frac{4(N_1 + N_2)\sigma_{12}\xi\alpha_x\alpha_y\alpha_z}{3\pi^2k_B} \times \frac{(T_1/2m_1 + T_2/2m_2)^{1/2}}{(T_1 + T_2\beta^{-2})^{3/2}} \quad (5)$$

For equal masses and trap frequencies we reproduce the result of Ref. [16].

For the initial conditions of our experiment we obtain an approximate initial cooling time constant, where we neglect the influence of the Cs temperature since Cs is much colder, heavier and more tightly confined than the Li.

$$\tau_{\text{init}}^{-1} = \frac{4(N_{\text{Li}} + N_{\text{Cs}})\sigma_{\text{LiCs}}\xi\alpha_x^{\text{Li}}\alpha_y^{\text{Li}}\alpha_z^{\text{Li}}}{3\pi^2k_B T_{\text{Li}}(2m_{\text{Li}})^{1/2}}. \quad (6)$$

In the final stage of sympathetic cooling the final temperature $\bar{T} = (N_1T_1 + N_2T_2)/(N_1 + N_2)$ is approached exponentially, with a time constant

$$\tau_f^{-1} = \frac{4\sqrt{2\xi}(N_1 + N_2)\sigma_{12}\alpha_x\alpha_y\alpha_z}{3\pi^2k_B\bar{T}(m_1 + m_2)^{1/2}} (1 + \beta^{-2})^{-3/2}. \quad (7)$$

The effect of the mass difference on the thermalization time is a factor $\xi^{-1/2} \sim 2.3$ in the time constant. At large mass difference, the thermalization efficiency *per collision* is reduced by a factor ξ , but the collision frequency depends on \bar{v} , which is proportional to $\xi^{-1/2}$.

5.2 Sympathetic evaporation

Under the circumstances in our experiment, we expect evaporation of the Li atoms especially during the first few collision times, as the initial Li energy distribution has a width comparable to the trap depth. Once the gases are thermalized, Li evaporation is exponentially suppressed, but still may occur due to the high Li-Cs collision rate. Cs evaporation is always strongly suppressed as the Cs trap depth is much larger than the relevant temperatures. We can approximately describe the regime of slow evaporation by assuming a truncated Boltzmann distribution [28] for the Li atoms. The number of evaporation events per second is the number of collisions multiplied by the probability that a collision leads to evaporation. For simplicity, we will neglect the position dependence of this probability. The evaporation flux in a two-component sample with a large mass ratio can be estimated from a detailed balance approach: The number of evaporation events is equal to the number of “atom capture” events that happen if the gas were in complete equilibrium with a distribution that extends above the trap edge ϵ_t . The latter number can be estimated for $\eta \equiv \epsilon_t/k_B T \gg 1$. We assume the dominant process is the one where a Li atom with an energy just above ϵ_t collides with a thermal Cs atom. The thermal motion of the Cs atom can be neglected if η is sufficiently large, and on average a fraction $\xi/2$ of the energy of the Li atom is transferred to the Cs atom. This leads to an estimate for the evaporation probability per collision of

$$P_{\text{evap}} \sim \exp(-\eta) \eta^2 \xi/4. \quad (8)$$

This estimate is good if $T_1 \sim T_2$, $2/\xi \gg 1$ and $\eta \gg 1$, and leads to an evaporation rate of $\Gamma_{\text{evap}} = \Gamma_{\text{col}} P_{\text{evap}}$. The amount of energy lost in an evaporation event is of order $\eta k_B T$, while the Cs atom that is involved in the last collision only loses a small amount of energy, of order $\eta \xi k_B T$. The Li distribution on the other hand loses a particle and an energy of $\sim \eta k_B T$, leading to a decrease of the mean energy per Li atom of

$$\Delta(e_{\text{Li}}) = \frac{\eta - 3/2 - \delta - \eta \xi k_B T}{N_{\text{Li}}}. \quad (9)$$

Here δ represents the average potential energy, $\delta = 0$ for a box potential and $\delta = 3/2$ for a harmonic trap. Since the evaporation cools the Li more than the Cs, we expect that evaporation leads to a small difference in mean energy between the two components, of order

$$\frac{e_{\text{Cs}} - e_{\text{Li}}}{\bar{e}} \approx e^{-\eta} \eta^2 \left(\eta - 3/2 - \delta - \frac{N_{\text{Li}} + N_{\text{Cs}}}{N_{\text{Cs}}} \eta \xi \right) / 4. \quad (10)$$

Here $\bar{e} = (N_{\text{Cs}} e_{\text{Cs}} + N_{\text{Li}} e_{\text{Li}}) / (N_{\text{Cs}} + N_{\text{Li}})$. The evaporation-induced energy difference is of the same order of magnitude as the difference in mean energy between a truncated Boltzmann distribution and the full thermal distribution described by the same temperature [28].

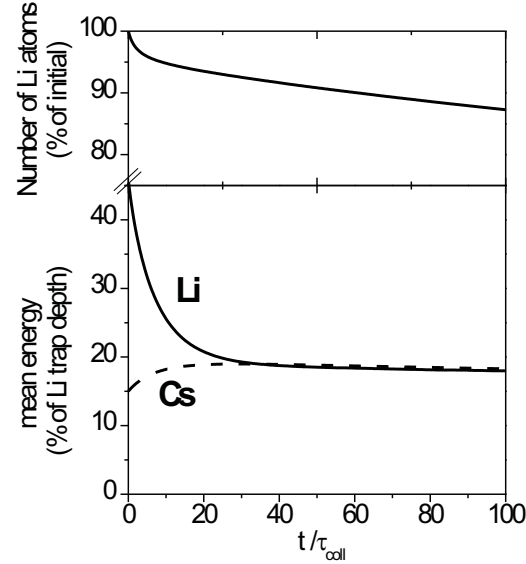


Fig. 7 Evolution of the particle number and internal energy in a simulated thermalization experiment. The number of Cs atoms is constant at 5 times the initial number of Li atoms. The mean energies cross over after 45 collisions, see text.

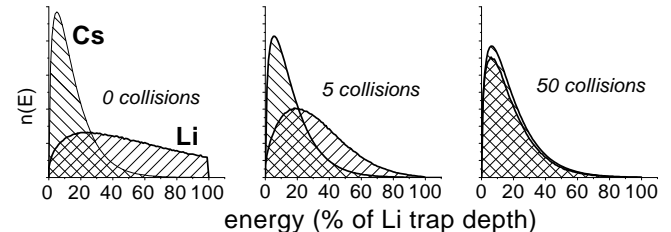


Fig. 8 Simulated evolution of the Li and Cs distributions. The left pane shows the initial Li distribution, which is a strongly truncated Maxwell-Boltzmann distribution. The Cs distribution is shown reduced in height by a factor 5.

5.3 Numerical simulation

The initial phase of thermalization, in which the distributions are strongly non-thermal, is difficult to describe in an analytical model. To obtain understanding of all phases of the thermalization process we made a numerical simulation of Li-Cs thermalization in a finite depth “box” potential well. We assume that due to the large scattering length the Cs distribution remains thermal at all times, while we numerically integrate the Boltzmann equation for the Li distribution. In Fig. 7 we show the evolution of the mean energies and particle numbers, where a broad initial distribution for the Li atoms was chosen. The evolution of the distributions is shown in Fig. 8.

In the initial phase of the thermalization process, the first ~ 5 collisions in Fig. 7, the Li has an internal energy per particle comparable to the trap depth, so that

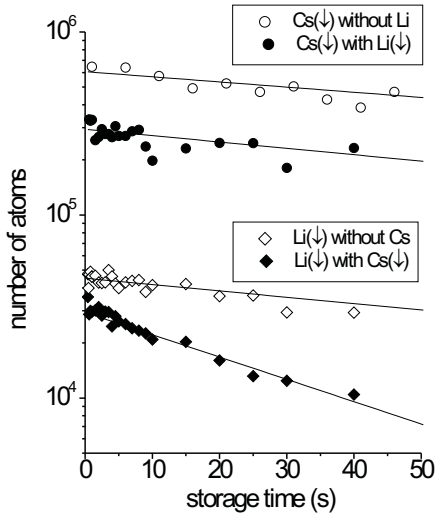


Fig. 9 Evolution of the number of trapped Li ($F=1$) and Cs ($F=3$) atoms in simultaneous trapping experiments (closed symbols). For comparison, the open symbols show the evolution of separately trapped gases. Thin lines: Exponential fits. Time constants are 150 s for Cs with or without Li, 125 s for Li without Cs, and 35 s for Li trapped simultaneously with Cs.

evaporation is very fast. After this rapid evaporation, a thermalization phase sets in (5 to 50 collisions) in which the mean energies rapidly converge. Finally, after 50 collisions a quasi-stationary phase with slow sympathetic evaporation and only slowly varying, almost equal temperatures sets in. We observe that although we start with $T_{\text{Li}} > T_{\text{Cs}}$, after ~ 50 collisions the evaporating Li gas has a lower average energy per particle than the Cs, reasonably well described by Eq.(10).

5.4 Comparison with measurements

A complete characterization of the thermalization process requires measurement of all relevant thermodynamic variables: the Li and Cs temperatures and particle numbers. Unfortunately, presently the Li temperature cannot be measured, and as $N_{\text{Cs}} \gg N_{\text{Li}}$, the effect of sympathetic cooling on the Cs temperature is too small to be measured accurately.

The evolution of the number of Li atoms in the trap is shown in Fig. 9. When stored separately, both Li and Cs gases decay due to rest gas collisions in 125 and 150 s respectively. There is no indication of evaporation in either case: Cs does not evaporate as its temperature is far below the trap depth. Li evaporation is energetically possible but the cross section for Li-Li collisions is so small that the characteristic timescale is > 1000 s.

When the gases are stored simultaneously, the Li atom number shows a non-exponential initial behavior followed by an approximately exponential decay with a

characteristic time of 35 s, which is much faster than the 125 s rest gas induced decay. We interpret the initial loss as due to evaporation in the first few Li-Cs collisions (cf. Fig. 7), and the slow decay as due to sympathetic evaporation after thermalization. Equation (8) now allows us to estimate the collision frequency. From the calculated Li trap depth and the measured Cs temperature after 20 s, $T_{\text{Cs}} = 44(5) \mu\text{K}$ we find $P_{\text{evap}} \sim 2 \times 10^{-3}$. This leads to an estimated collision rate per Li atom of $\sim 14 \text{ s}^{-1}$, and finally through Eq.(4) we find the estimated cross section

$$\sigma_{\text{CsLi}} \sim 5 \times 10^{-12} \text{ cm}^2. \quad (11)$$

From the collision rate we infer a cross-species thermalization time of approximately 1 s, which is much shorter than the rest gas limited storage times in our trap. Therefore, we conclude that sympathetic cooling of Li by Cs is a viable method to produce ultracold Li gas.

6 Conclusion

In conclusion, we have simultaneously stored ultracold lithium and cesium atoms in a conservative optical dipole trap. Exoergic spin-changing collisions lead to trap loss on a time scale of a few seconds at densities of 10^{10} atoms/cm³ and 10^{12} atoms/cm³ for lithium and cesium, respectively. Under conditions where exoergic collisions are impossible, a slow loss of Li atoms is observed, which we attribute to sympathetic evaporation through elastic Li-Cs collisions. The interpretation in terms of a model for sympathetic cooling and evaporation provides an estimated cross-thermalization time of one second.

The interpretation of the observations in terms of sympathetic cooling should be confirmed by measurements of the temperature evolution and phase space density. Such measurements are currently in preparation. Temperature data will also enable us to measure the elastic cross section σ_{CsLi} for cold, elastic Li-Cs collisions more accurately. Optimization of the Cs cooling process is certainly possible and will lead to lower final temperatures of the Li gas.

Repeated pulsed optical cooling of the Cs may be useful to remove thermal energy from the system without loss of atoms. This method offers a possible route towards quantum degeneracy of Li without evaporation. The de Broglie wavelength of Li is larger than that of Cs at the same temperature by a factor of 4.4, which makes it possible to achieve quantum degeneracy with either the fermionic or the bosonic Li isotopes in thermal contact with optically cooled Cs. For 10^6 Li atoms in our trap we find a degeneracy temperature $T_{\text{deg}} \simeq \hbar(\omega_x \omega_y \omega_z N_{\text{Li}})^{1/3} / k_B = 3 \mu\text{K}$, well within the range of standard optical cooling techniques for Cs. But even at the temperatures we reach presently, sympathetic cooling significantly increases the Li density in the centre of the trap. This is an essential step towards creation

of cold heteronuclear molecules, as all proposed formation mechanisms, in particular photoassociation, rely on a high pair densities of the two species.

Acknowledgements

This work has been supported in part bei the Deutsche Forschungsgemeinschaft. A.M. is supported by a Marie-Curie fellowship from the European Community programme IHP under contract number CT-1999-00316. We are indebted to D. Schwalm for encouragement and support. We thankfully acknowledge many fruitful discussions with A.N. Salgueiro and H.A. Weidenmüller.

References

1. J. Stenger *et al.*, *Nature* **396**, 345 (1998).
2. H. Pu and N.P. Bigelow, *Phys. Rev. Lett.* **80**, 1130 (1998); *ibid.*, 1134 (1998).
3. K. Mølmer, *Phys. Rev. Lett.* **80**, 1804 (1998); E. Timmermans and R. Coté, *ibid.*, 3419 (1998); H. Heiselberg *et al.*, *ibid.* **85**, 2418 (2000).
4. He Wang and W.C. Stwalley, *J. Chem. Phys.* **108**, 5767 (1998).
5. H.F. Hess *et al.*, *Phys. Rev. Lett.* **59**, 672 (1998); R. van Roijen, *et al.*, *ibid.* **61**, 931 (1988).
6. J.D. Weinstein *et al.*, *Nature* **395**, 148 (1998).
7. C.J. Myatt *et al.*, *Phys. Rev. Lett.* **78**, 586 (1997).
8. B. DeMarco and D.S. Jin, *Science* **285**, 170 (1999).
9. I. Bloch *et al.*, *Phys. Rev. A* **64**, 021402 (2001).
10. F. Schreck *et al.*, *Phys. Rev. A* **64**, 011402 (2001).
11. A. G. Truscott *et al.*, *Science* 291: 2570 (2000).
12. G. D. Telles *et al.*, *Phys. Rev. A* **62**, 033406 (2001), and references therein.
13. Y. E. Young *et al.*, *Phys. Rev. A* **62**, 055403 (2000), and references therein; J. P. Schaffer, W. Chalupczak, and N. P. Bigelow, *Phys. Rev. A* **60**, R3365 (1999).
14. U. Schlöder *et al.*, *Eur. Phys. J. D* **7**, 331 (1999).
15. S.D. Gensemer *et al.*, *Phys. Rev. A* **62**, 030702 (2000).
16. G. Delannoy *et al.*, *Phys. Rev. A* **63**, 051602R (2001).
17. T. Takekoshi and R.J. Knize, *Opt. Lett.* **21**, 77 (1996).
18. R. Grimm, M. Weidemüller, Yu.B. Ovchinnikov, *Adv. At. Mol. Opt. Phys.* **42**, 95 (2000).
19. A. Hemmerich *et al.*, *Phys. Rev. Lett.* **75**, 37 (1995); D. Boiron *et al.*, *Phys. Rev. A* **52**, R3425 (1995).
20. W. Ketterle, D.S. Durfee and D.M. Stamper-Kurn, in: *Proc. of the International School of Physics - Enrico Fermi*, ed. by M. Inguscio, S. Stringari, C.E. Wieman (IOS Press, Amsterdam 1999), p. 67.
21. T.A. Savard, K.M. O'Hara, and J.E. Thomas, *Phys. Rev. A* **56**, R1095 (1997).
22. H. Engler *et al.*, *Phys. Rev. A* **62**, 031402(R) (2000).
23. U. Schünemann *et al.*, *Opt. Comm.* **158**, 263 (1998).
24. I.F. Silvera and J.T.M. Walraven, in: *Progress in Low Temperature Physics Vol. 44*, ed. by D.F. Brewer (North-Holland, Amsterdam 1986), 139.
25. J. Weiner *et al.*, *Rev. Mod. Phys.* **71**, 1 (1999).
26. M. Lewenstein, J.I. Cirac, and P. Zoller, *Phys. Rev. A* **51**, 4617 (1995).
27. T. Papenbrock, A.N. Salgueiro, and H.A. Weidenmüller, submitted to *Phys. Rev. Lett.*; arXiv: cond-mat/0106392.
28. O. J. Luiten *et al.*, *Phys. Rev. A* **53**, 381 (1996); P. W. H. Pinkse *et al.*, *Phys. Rev. A* **57**, 4747 (1998).